INTERNATIONAL JOURNAL OF CLIMATOLOGY
Int. J. Climatol. **24**: 1625–1644 (2004)
Published online in Wiley InterScience (www.interscience.wiley.com). DOI: 10.1002/joc.1094

TREND AND VARIABILITY OF CHINA PRECIPITATION IN SPRING AND SUMMER: LINKAGE TO SEA-SURFACE TEMPERATURES

FANGLIN YANG[a,*] and K.-M. LAU[b]
[a] *GEST/UMBC, Climate and Radiation Branch, NASA Goddard Space Flight Center, Greenbelt, MD 20771, USA*
[b] *Laboratory for Atmospheres, NASA Goddard Space Flight Center, Greenbelt, MD 20771, USA*

Received 16 May 2003
Revised 21 July 2004
Accepted 21 July 2004

ABSTRACT

Observational records in the past 50 years show an upward trend of boreal-summer precipitation over central eastern China and a downward trend over northern China. During boreal spring, the trend is upward over southeastern China and downward over central eastern China. This study explores the forcing mechanism of these trends in association with the global sea-surface temperature (SST) variations on the interannual and interdecadal time scales.

Results based on singular value decomposition (SVD) analyses show that the interannual variability of China precipitation in boreal spring and summer can be well defined by two centres of action for each season, which are covarying with two interannual modes of SSTs. The first SVD modes of precipitation in spring and summer, which are centred in southeastern China and northern China respectively, are linked to an El Niño–southern oscillation (ENSO)-like mode of SSTs. The second SVD modes of precipitation in both seasons are confined to central eastern China, and are primarily linked to SST variations over the warm pool and the Indian Ocean. Features of the anomalous 850 hPa winds and 700 hPa geopotential height corresponding to these modes support a physical mechanism that explains the causal links between the modal variations of precipitation and SSTs.

On the decadal and longer time scale, similar causal links are found between the same modes of precipitation and SSTs, except for the case of springtime precipitation over central eastern China. For this case, while the interannual mode of precipitation is positively correlated with the interannual variations of SSTs over the warm pool and Indian Ocean, the interdecadal mode is negatively correlated with a different SST mode, i.e. the North Pacific mode. The latter is responsible for the observed downward trend of springtime precipitation over central eastern China. For all other cases, both the interannual and interdecadal variations of precipitation can be explained by the same mode of SSTs. The upward trend of springtime precipitation over southeastern China and downward trend of summertime precipitation over northern China are attributable to the warming trend of the ENSO-like mode. The recent frequent summertime floods over central eastern China are linked to the warming trend of SSTs over the warm pool and Indian Ocean. Copyright © 2004 Royal Meteorological Society.

KEY WORDS: East Asian monsoon; precipitation; sea-surface temperature; interannual and interdecadal variability

1. INTRODUCTION

Precipitation over China exhibits complex space and time structures. Large interannual variability causes local precipitation to fluctuate from year to year. Severe floods and droughts often occur in the same season of a year over different regions. For example, in the summer of 1997, southern China was flooded with excessive rainfall, while northern China faced one of the severest droughts on record (Huang *et al*., 2000; Lau and Weng, 2001). On the decadal and longer time scale, persistent dry and wet conditions have been observed over certain regions (e.g. Weng *et al*., 1999; Chang *et al*., 2000; Hu *et al*., 2003). During the second half of last century, northern China received abundant rainfall in the 1950s and suffered severe drought in the 1970s

* Correspondence to: Fanglin Yang, Climate and Radiation Branch, NASA Goddard Space Flight Center, Code 913, Greenbelt, MD 20771, USA; e-mail: fyang@climate.gsfc.nasa.gov

and 1980s. Over central eastern China, an upward trend of precipitation was observed in boreal summer and a downward trend in boreal spring. Over southern China, precipitation has been increasing in boreal spring and decreasing in boreal summer.

Precipitation over China has distinct seasonal characteristics, and is largely controlled by the monsoon circulation. Traditionally, the time from mid-May to the end of August has been defined as the East Asian summer monsoon season (Tao and Chen, 1987). The heaviest rainfall often occurs in mid-June over the Yangtze River and Huaihe River valleys. For this reason, earlier studies have focused almost exclusively on the June–July–August (JJA) season in the investigations of Asian precipitation variability and trends (e.g. Ding, 1992; Nitta and Hu, 1996; Hu ZZ, 1997; Lau and Yang, 1997; Chang *et al*., 2000; Wang *et al*., 2001; Lau and Weng, 2001; Gong and Ho, 2002; Wu, 2002). Little attention has been paid to precipitation in the March–April–May (MAM) season. Our analysis (see Figure 1), however, indicates that over southern China (south of the Yangtze Rive), on average, precipitation in each of MAM and JJA accounts for about 35% of the annual total. Over southeastern China, the rainy season starts as early as March. Precipitation in each of the months of MAM accounts for about 10% of the annual total. Given the possibility that rainfall anomalies in MAM may precede those in JJA, in the present study we investigate the variability and trends of China precipitation in both the MAM and JJA seasons.

Precipitation over China is affected by both the internal dynamics of the monsoonal circulation and external forcing (Webster *et al*., 1998). A few major external forcing factors have been identified in previous studies to be influential on the variability of China precipitation, such as sea-surface temperatures (SSTs), Tibetan Plateau heating, Eurasian snow cover, and polar ice coverage. Among them, the influence of SSTs has been explored to the greatest extent. Most of the investigations have focused on the relation between China precipitation in boreal summer and the El Niño–southern oscillation (ENSO) events, mainly because of the overwhelming effects of ENSO on the climate system at the global scale. However, how ENSO events influence China summer precipitation is still not conclusive. Correlation between the eastern Pacific SST

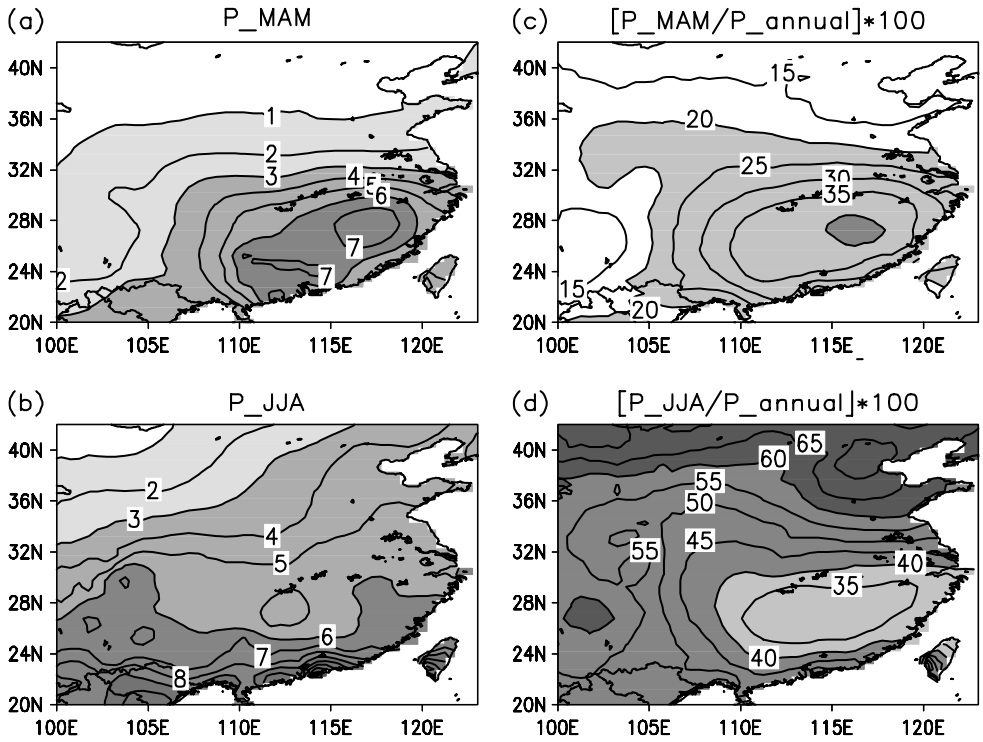

Figure 1. Seasonal mean precipitation (mm/day) in (a) MAM and (b) JJA averaged for the 1951–98 period, and the percentage of seasonal mean precipitation relative to the annual total for (c) MAM and (d) JJA

anomalies and China summer monsoon is weak, and not statistically significant (Chen *et al*., 1992). Wang *et al*. (2000) proposed a Pacific–East Asia teleconnection mechanism to explain the ENSO effect on East Asian climate. This mechanism emphasizes the importance of air–sea interaction over the Philippine Sea in modulating the strength and location of the western North Pacific anticyclone. In addition to the SSTs in the tropical central and eastern Pacific that are dominated by ENSO variability, SSTs over other oceanic regions, such as the Kuroshio Current, the western Pacific warm pool, the South China Sea and the Indian Ocean, have also been found to be influential on the East Asian summer monsoon (e.g. Huang and Lu, 1989; Shen and Lau, 1995; Nitta and Hu, 1996; Wu *et al*., 2003). Instead of focusing on SSTs in a particular region, we include in the present study the SSTs over the Indian Ocean and Pacific Ocean north of 30 °S. The covariance matrix built on the seasonal mean precipitation anomalies over eastern China and SST anomalies over the two oceanic basins is analysed for each season in MAM and JJA using the singular value decomposition (SVD) technique (Bretherton *et al*., 1992) to search for coupled patterns of precipitation and SSTs that are covarying in time. This technique is capable of finding the SSTs over different oceanic regions that may possess a collective effect on a certain mode of precipitation over China.

Weng *et al*. (1999) investigated the coupled variability of precipitation over China and global SSTs in boreal summer. They applied SVD to the unfiltered precipitation and SSTs and discovered a few dominant precipitation modes that are covarying with SSTs at multiple time scales ranging from interannual to interdecadal. We take a different approach in the present study, assuming that the modes of precipitation at the interannual and decadal time scales are not necessarily the same and that they might be forced by different modes of SSTs. This approach also enables us to examine how the interannual and decadal components interplay. As will be shown later, the variability of at least one mode of precipitation at different time scales is linked to different modes of SSTs. In addition, the present study differs from Weng *et al*. (1999) in a few other aspects. We included both the MAM and JJA seasons and utilized different observational datasets. Considering the scarcity and quality of observations over western China, our investigation is limited to eastern China (east of 105 °E) instead of the entire country.

The purpose of the present study is to document the variability of China precipitation in boreal spring and summer, and its links to the variations of global SSTs at different oceanic regions and at different time scales. The possibility that the observed trends of China precipitation in the past 50 years were forced by interdecadal SST variations is explored. For this purpose, we analyse first the basic features of the observed precipitation over East China (Section 2) and the coupled modes of precipitation and SSTs at the interannual time scale (Section 3). Attempts are made in Section 4 to connect these modes with the anomalous large-scale circulation and height field. Section 5 investigates the trends and decadal variability of the observed precipitation, and their possible links to the decadal variations of SSTs. Section 6 summarizes our findings and discusses issues that call for further investigation.

2. OBSERVED TRENDS AND VARIABILITY

This section documents basic features of the observed precipitation over China and global SSTs. The analysis is based on the New *et al*. (2000) precipitation and the NOAA extended reconstructed SSTs datasets. The former has a resolution of $0.5^\circ \times 0.5^\circ$ and covers the time from 1901 to 1998. The SST dataset was provided by the NOAA–CIRES Climate Diagnostics Center, Boulder, CO, USA, from their Website at http://www.cdc.noaa.gov/. It has a resolution of $2^\circ \times 2^\circ$ degrees and covers the time from 1854 to the present. The present investigation focuses on the period from 1951 to 1998 to take advantage of the better quality of data after 1950 and the availability of the National Centers for Environmental Prediction (NCEP)–National Center for Atmosphere Research (NCAR) reanalysis (Kalnay *et al*., 1996) after 1948. We have extended the analyses, where data permit, back to 1901, and also repeated the investigation for the 1951–98 period using another independent gridded land precipitation product (Chen *et al*., 2002). We came to the same qualitative conclusion. Weng *et al*. (1999) investigated the summertime precipitation variability over China based on meteorological station data over a slightly different domain. The dominant modes of summertime precipitation found in the present study are, by and large, the same as those documented by Weng *et al*.

(1999). Therefore, we feel confident that the results obtained in the present study should be robust and not sensitive to the type and length of data used.

Figure 1 depicts the 1951–98 averaged seasonal mean precipitation for the MAM and JJA seasons, and the percentages of seasonal mean precipitation relative to the annual total. In MAM, heavy precipitation is confined to the south of the Yangtze River and concentrated over the southeast, reaching up to 7.0 mm/day. In JJA, the precipitation band extends to northern China, with the rates decreasing gradually from south to north. Over southeastern China, precipitation in each of MAM and JJA accounts for about 35% of the annual total. Over central eastern China along the Yangtze Rive and Huaihe River valleys, precipitation in MAM accounts for about 20–30% of the annual total, and in JJA about 40–50%. Over northern China, precipitation is concentrated in the JJA season, accounting for more than 60% of the annual total. Previous studies have focused primarily on the summertime precipitation (e.g. Huang and Wu, 1989; Weng *et al*., 1999; Chang *et al*., 2000; Lau and Weng, 2001; Wang *et al*., 2001). Figure 1 reveals that, over southeastern and central eastern China, precipitation in MAM is as important as that in JJA. This fact motivated us to examine precipitation in both the seasons.

The trends of precipitation in JJA over central and northern China in recent decades have been documented in a few earlier studies (e.g. Weng *et al*., 1999; Chang *et al*., 2000), and have prompted debate on its causes (e.g. Gong and Ho, 2002; Menon *et al*., 2002). In the present study, precipitation trends are detected in both the JJA and MAM seasons. Figure 2 displays the differences between the means of precipitation averaged for the 1975–98 period and the 1951–74 period in each season. Consistent with earlier findings, in JJA the precipitation exhibits an upward trend over central eastern China and a downward trend over northern China. In contrast, in MAM, an upward trend over southeastern China and a downward trend over central eastern China are detected. Interestingly, the MAM and JJA trends are almost opposite to each other in geographical locations. To illustrate further how precipitation over different regions has varied from year to year, we divided East China into three regions, i.e. southern China (110–122 °E, 21–28 °N), central China (110–122 °E, 28–33 °N) and northern China (110–122 °E, 33–40 °N). Mean precipitation anomalies over each section were computed for the years from 1951 through to 1998 for each season. The anomaly at each grid point was predefined as the departure from the 1951–98 seasonal mean. Figure 3 shows the time evolution of the means over southern China and central China for MAM and the means over central China and northern China for JJA. A 7 year running mean is also added to each bar graph to illustrate decadal variations and long-term trends. The time series for all regions and in both seasons show large interannual and decadal variations. A switch of the anomaly sign around the mid 1970s is prominent for all cases. In MAM, southern China was very dry in the 1960s and wet in the 1980s. In JJA, central China experienced frequent droughts in the 1950s and frequent floods in the late 1990s, and a general upward trend of precipitation starting in the 1960s. Interdecadal variation is evident. For northern China in JJA, it was rather wet in the 1950s and

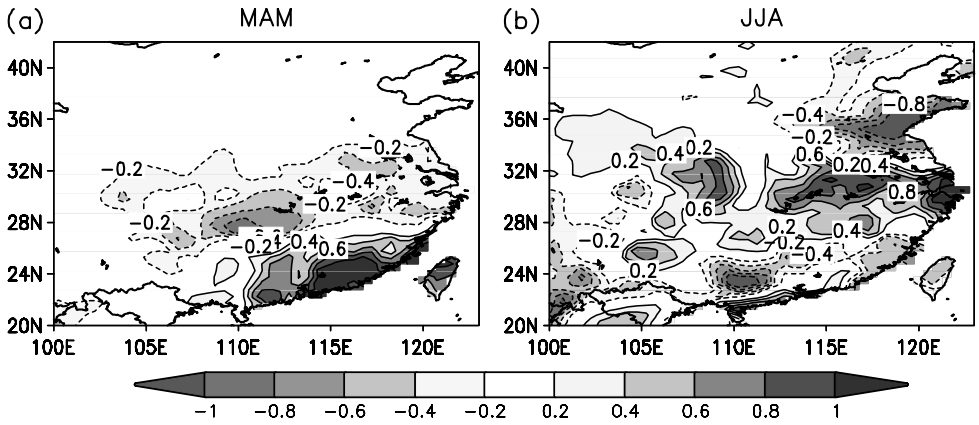

Figure 2. Differences of seasonal mean precipitation (mm/day) between the 1975–98 average and the 1951–74 average for (a) MAM and (b) JJA

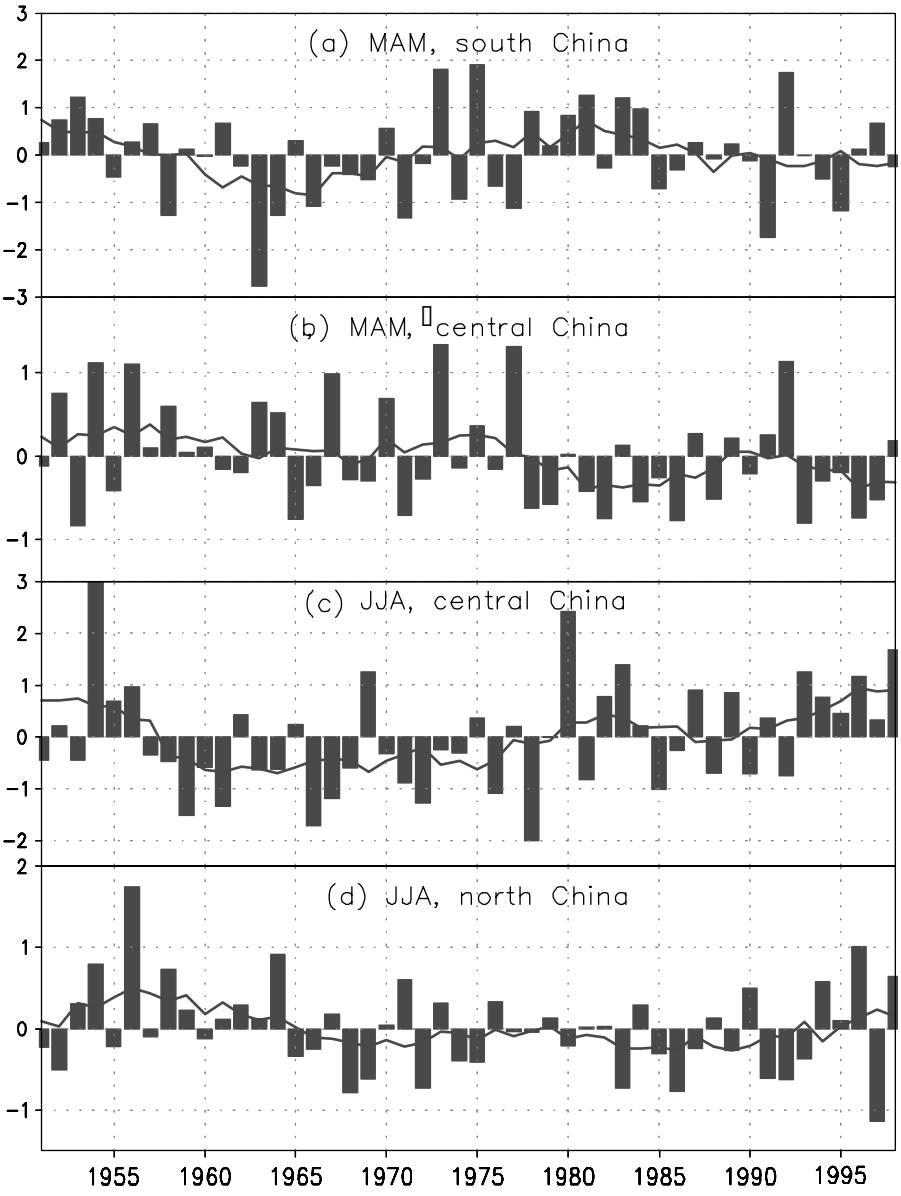

Figure 3. Regional and seasonal mean precipitation anomalies (mm/day) shown as bars for (a) MAM over southern China, (b) MAM over central China, (c) JJA over central China and (d) JJA over northern China. The line in each panel shows the 7 year running means of the bars, and depicts the decadal variation of the regional mean precipitation. The regions are defined in the text. Precipitation anomalies are computed at each grid point before regional means are derived. The anomaly at each grid point is defined as the departure from the 1951–98 seasonal mean

early 1960s, and extremely dry in the 1980s. In late 1990s, the drought situation over northern China was somewhat alleviated, though 1997 summer was the driest in the record. Lau and Weng (2001) found that the 1997 drought over northern China and the 1998 flood over central China were triggered by the 1997–98 El Niño event.

The trend and variability of global SSTs have been documented in detail in many studies (e.g. Zhang *et al*., 1997; Xue *et al*., 2003). For illustration purposes, we present in Figure 4 the differences in seasonal mean SSTs between the 1975–89 and 1951–74 periods for both MAM and JJA over the domain (30 °S–60 °N,

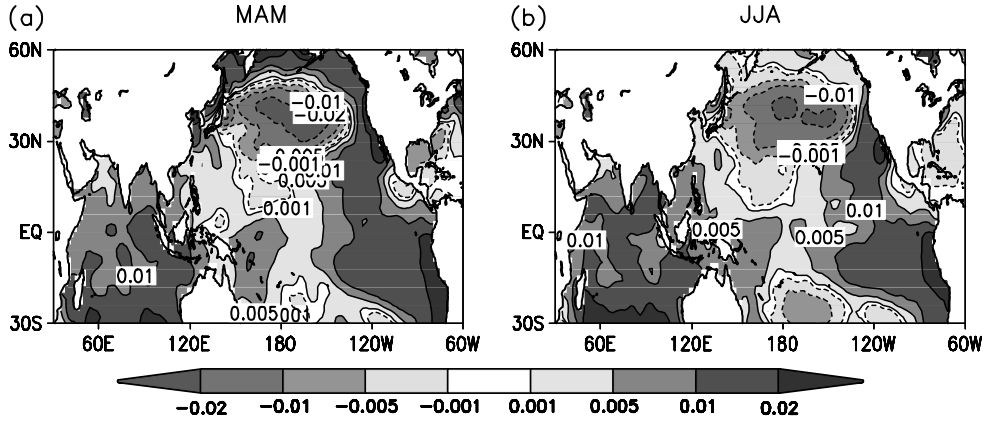

Figure 4. As Figure 2, except for SSTs

30 °E–60 °W). The SST patterns are similar for both seasons, indicating upward trends over the central and eastern tropical Pacific and tropical Indian Ocean, and downward trends over the central to western North Pacific. Are the trends of China precipitation linked to the trends of global SSTs? Are the relations between China precipitation and global SSTs on the interannual time scale different from that on the decadal time scale? These questions are addressed in the following sections.

3. COHERENT MODES OF PRECIPITATION AND SSTS ON AN INTERANNUAL TIME SCALE

SVD is used in this section to identify coupled modes of variability between precipitation and SSTs. SVD (Bretherton *et al*., 1992) decomposes the cross-covariance matrix of two data fields and identifies the pairs of spatial patterns that explain the mean-squared temporal covariance between the two fields. It can explain the maximum possible fraction of the cumulative squared covariance with fewer leading modes than any other tool that is capable of isolating coupled modes of variability between the time series of two fields. It should be pointed out that, due to its limitations, the SVD, under certain circumstances, may produce paired patterns of no physical meaning (Newman and Sardeshmukh, 1995; Cherry, 1997; Hu Q, 1997). Cherry (1997) suggests that, prior to the use of SVD, one should apply empirical orthogonal function (EOF) analysis to each field to test whether the two sets of expansion coefficients from EOF analysis are strongly correlated and the patterns are geophysically relevant. We carried out EOF analyses on the precipitation and SST fields and found that such conditions were met. Newman and Sardeshmukh (1995) suggest, from a different perspective, that SVD modes are physically meaningful only if they explain significant portions of the variance of their respective fields. The percentage variances explained by the first two leading modes from our SVD analyses (see Tables I and II) are, by and large, significant. Thus, it is appropriate and advantageous to utilize the SVD technique in this study.

Weng *et al*. (1999) and Lau and Weng (2001) investigated the coupled modes between China precipitation and global SSTs in boreal summer. They applied SVD to the observed precipitation from 1954 to 1998 at all meteorological stations in China and a global SST dataset that is different from what we used here. Considering the scarcity of observations over western China, we focused our investigation on eastern China, but included the spring season. In addition, a digital filter (Duchon, 1979) with a cutoff period of 7 years was utilized to extract the high- and low-frequency components from the observed seasonal mean anomalies. The SVD analysis was applied to the high-frequency component. Consequently, the coupled modes of precipitation and SSTs identified by the SVD analysis explain only the variability on the interannual time scale. This approach enables us to examine how the interannual and decadal components interplay.

We performed SVD analyses using the 7 year high-frequency-pass filtered datasets of precipitation over East China (21–42 °N, 105–122 °E) and SSTs in the Pacific and Indian Ocean north of 30 °S, for the MAM

Table I. Percentage variances of SST, precipitation and the SST–precipitation covarying matrix explained by the leading SVD modes, and the correlations between the PCs of SST and precipitation. Results are based on 7 year high-frequency-pass filtered data

	SST variance (%)	Precipitation variance (%)	SST–precipitation covariance (%)	Correlation (PC_sst, PC_precip)
MAM				
SVD 1	31	27	27	0.57
SVD 2	11	15	14	0.64
JJA				
SVD 1	43	10	24	−0.77
SVD 2	7	17	13	0.76

Table II. As Table I, except that the SVD analysis was performed using unfiltered data

	SST variance (%)	Precipitation variance (%)	SST–precipitation covariance (%)	Correlation (PC_sst, PC_precip)
MAM				
SVD 1	34	25	28	0.55
SVD 2	7	16	11	−0.61
JJA				
SVD 1	33	9	19	−0.66
SVD 2	6	18	12	0.70

and JJA seasons and for the years from 1951 to 1998. The percentage variances of the individual SST and precipitation fields and the fractional variance of the SST–precipitation covarying matrix explained by the first two leading SVD modes are listed in Table I, together with the correlations between the principal components (PCs) of the SST and precipitation modes. The first two leading modes of SST and precipitation for both the MAM and JJA seasons are presented in Figure 5 as homogeneous correlation maps. The SST (precipitation) homogeneous correlation map depicts the correlation between the filtered SST (precipitation) anomaly at each grid point and the leading-mode PC of SSTs (precipitation). At each grid point, the square of the correlation measures the percentage variance explained by the corresponding mode. Correlations larger than 0.36 in magnitude are statistically significant at the 99% level using a Student's t-test.

In MAM, the first SST mode (Figure 5(a)) is a typical ENSO-like mode, with positive anomalies in the central and eastern tropical Pacific and Indian Ocean, and a horseshoe shape of negative anomalies in the tropical western Pacific. The covarying precipitation mode (Figure 5(e)) explains more than 60% of the local precipitation variance over southeastern China. The first SVD mode explains 31% SST variance, 27% precipitation variance and 27% fractional variance of the SST–precipitation covarying matrix. The PCs of SST and precipitation are positively correlated ($r = 0.57$). This implies that southeastern China tends to have more precipitation in years when the central and eastern tropical Pacific and Indian Ocean are abnormally warm in MAM. The second SST mode in MAM (Figure 5(b)) reflects SST variations over the warm pool and Indian Ocean and, to a lesser degree, over the eastern North Pacific. Precipitation over central eastern China is positively correlated to the PC of SSTs (Figure 5(f)). The second SVD mode explains 11% SST variance, 15% precipitation variance and 14% fractional variance. The correlation between the PCs of SST and precipitation is 0.64. In non-ENSO years, when the western tropical Pacific and Indian Ocean are abnormally warm (cold) in MAM, central eastern China tends to have more (less) precipitation.

In JJA, the first SST mode also exhibits a typical ENSO-like mode (Figure 5(c)), and explains 43% of its own variance. Precipitation over northern China is highly correlated with this mode of SSTs. The correlation between the PCs of precipitation and SSTs reaches −0.77. Such a negative relationship between the tropical

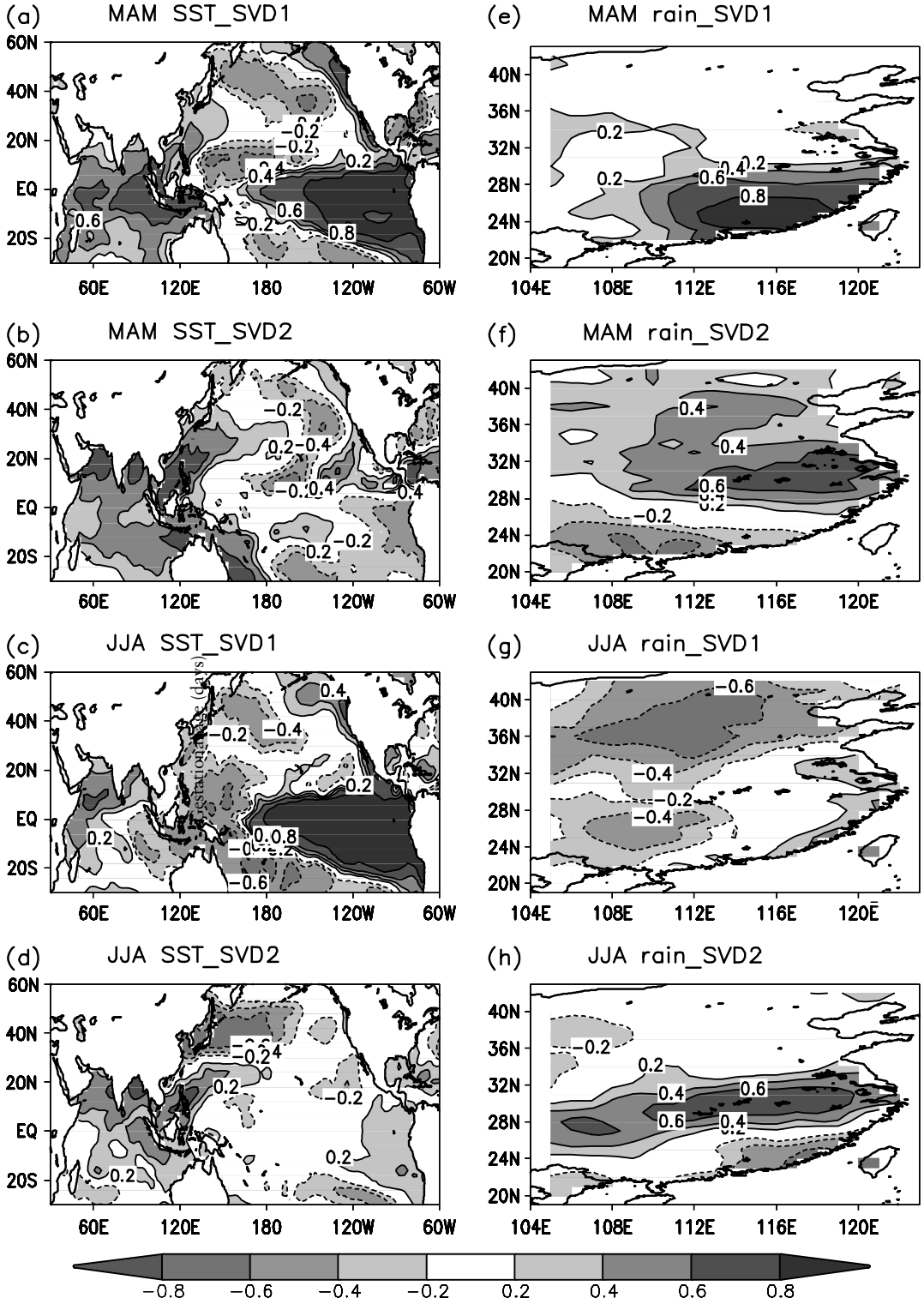

Figure 5. First two leading SVD modes of SSTs (left panels) and precipitation (right panels) for MAM (upper four panels) and JJA (lower four panels). These modes are derived from 7 year high-frequency-pass filtered precipitation and SSTs, and are shown as homogeneous correlation maps

central and eastern Pacific SSTs and the northern China precipitation has been confirmed by both atmospheric general circulation model (GCM) simulations and observational data analyses (e.g. Wang and Li, 1990; Ju and Slingo, 1995; Weng *et al*., 1999; Chang *et al*., 2000). In years when SSTs in the central and eastern tropical Pacific are abnormally warm, East Asian monsoon circulation tends to be weak and the monsoon onset is usually delayed. This results in less precipitation in late summer over northern China. The second SVD modes of SSTs and precipitation in JJA (Figure 5(d) and (h)) show that over central eastern China the interannual variation of precipitation is correlated with a north–south dipole mode of SST anomalies over the western North Pacific, the tropical Indian Ocean and the warm pool. This SVD mode explains 7% SST variance, 17% precipitation variance and 13% fractional variance. The PCs of precipitation and SST are positively correlated ($r = 0.76$). In years when SSTs over the warm pool and northern Indian Ocean are abnormally warm and SSTs over the western North Pacific abnormally cold, precipitation over central eastern China tends to be heavier than usual.

4. ANOMALOUS WINDS AND HEIGHT

In Section 3, certain causal links were identified between the principal modes of precipitation over East China and the main variations of global SSTs. In this section we investigate the characteristics of the atmospheric circulation corresponding to these modes. The data used are the NCEP–NCAR reanalysis from 1951 through to 1998 (Kalnay *et al*., 1996). We analysed seasonal-mean zonal and meridional winds at 850 hPa and geopotential height at 700 hPa.

Wu *et al*. (in press) discovered large discrepancies of decadal changes of sea-level pressure and mid-tropospheric height in the Asian region between the NCEP–NCAR reanalysis and observations. To minimize the impact of data discrepancy, and also to be consistent with the SVD analysis that deals only with the interannual variability of precipitation and SSTs, all wind and height data were high-pass filtered (Duchon, 1979) to truncate the low-frequency components with periods longer than 7 years. Then, the filtered winds and height at each grid point are regressed against the leading PCs of precipitation and SST respectively. The regressions are shown in Figure 6 as anomalous wind vectors at 850 hPa and anomalous geopotential heights at 700 hPa, with respect to one standard deviation of each PC. For both seasons and for all modes, the regressions to the PCs of precipitation resemble those to the PCs of SSTs in terms of pattern distribution, since the PCs of precipitation and SSTs are highly correlated (see Table I). For each PC, we also computed the composites of anomalous winds and height for extreme events with the PC greater or smaller than one standard deviation (not shown). The resulting composites of wind and height anomalies are in agreement with those derived from the regression analyses.

In MAM, the regressions to the first-mode PC of SSTs (Figure 6(a)) and precipitation (Figure 6(e)) both show positive height anomalies in the subtropics and negative anomalies in the mid-latitude western Pacific. Anomalous geostrophic flow enhances the climate-mean southeast winds over southeastern China. In combination with Figure 5(a) and (e) a picture emerges of how the anomalous SSTs influence the springtime precipitation over southern China. In years when the SSTs in the central and eastern tropical Pacific and Indian Ocean are above normal, SSTs in the western tropical Pacific are usually below normal (Figure 5(a)). The western Pacific subtropical high tends to remain in the south. As a result, abnormally strong southeast winds along the edge of the subtropical high bring more warm and moist air, and hence more precipitation over southeastern China. The opposite is true for the negative phase of the SST mode.

The regressions to the second-mode PC of SSTs (Figure 6(b)) and precipitation (Figure 6(f)) in MAM indicate that, when above-normal SSTs exist over the warm pool and northern Indian Ocean (Fig. 5b), the western Pacific subtropical high is abnormally strong and is shifted northward. The height anomalies over northern Eurasia are negative. Stronger south and southeast flows along the west edge of the subtropical high bring abundant warm and moist air to central eastern China. A convergence zone forms, and above-normal precipitation occurs downstream of the Yangtze Rive valley (Figure 5(f)).

In JJA, precipitation over northern China is negatively correlated with the ENSO-like SST mode; hence there is a negative correlation between the first-mode PCs (Table I). For clarity, we have reversed the sign

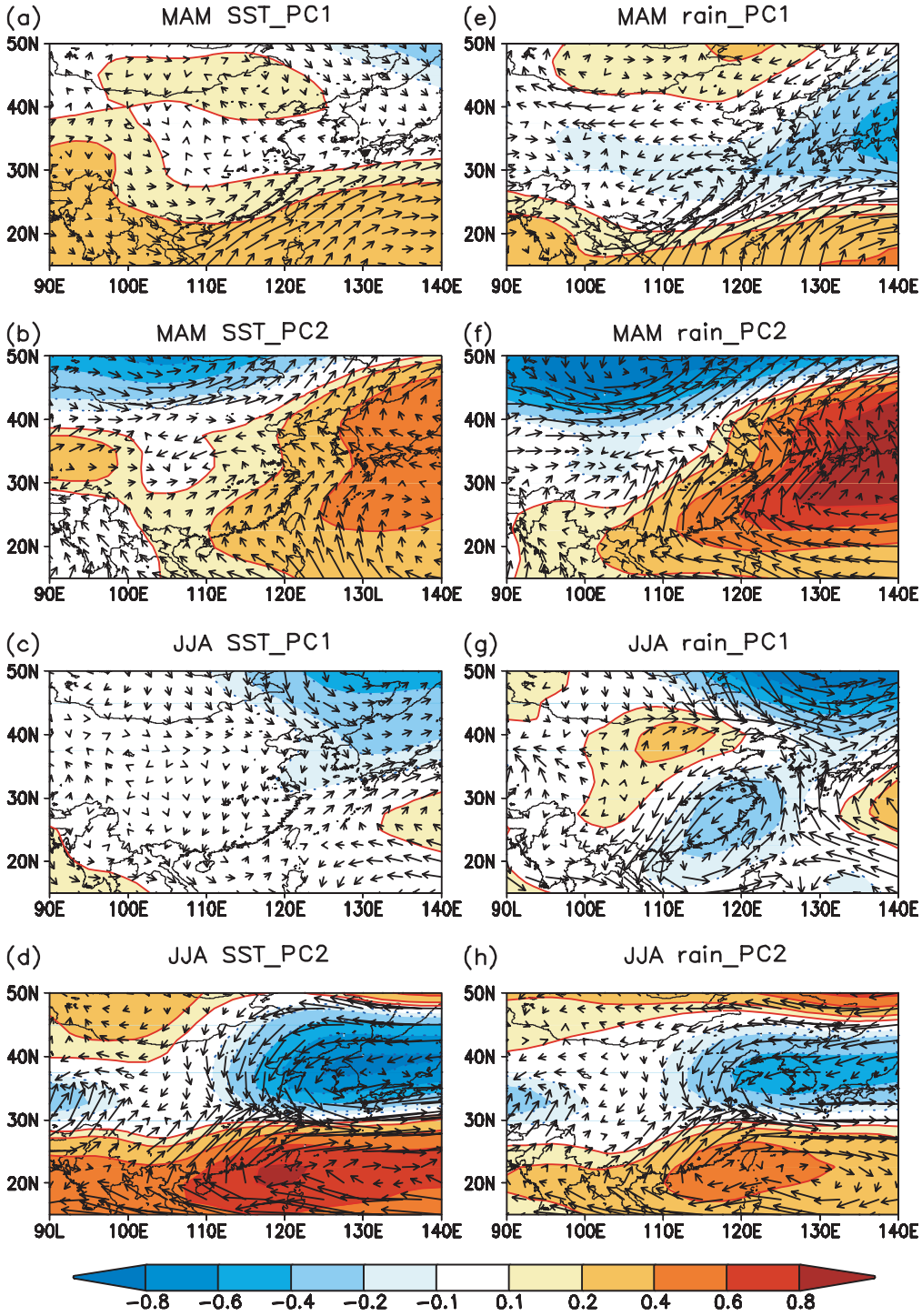

Figure 6. Regressions of 850 hPa zonal and meridional winds and 700 hPa geopotential height against the PCs of the SVD modes shown in Figure 5. Left panels are for the regressions against the PCs of SSTs, and right panels for those against the PCs of precipitation. The winds and height data are filtered to exclude variations with period longer than 7 years. The resulting anomalous winds (m/s) are shown in each panel as vectors, and anomalous geopotential height (m) is shaded. Note that for JJA the sign of rain_PC1 was reversed before regression because it is negatively correlated with SST_PC1. This figure is available in colour online at http://www.interscience.wiley.com/ijoc

of the PC for precipitation for regression analysis. The results (Figure 6(c) and (g)) indicate that the western Pacific subtropical high tends to retreat to the east in years when the SSTs are abnormally warm in the central and eastern tropical Pacific and cold in the western tropical Pacific, a typical ENSO-like mode. Anomalous low-level southwesterly flow weakens the normal southeast monsoon winds along the edge of the subtropical high over central and northern China in the summer months. Moreover, an anomalous low occurs over northeastern China. The anomalous cyclonic flow over northern China brings dry and cold air to northeastern China. As a result, the monsoon precipitation over northern China is suppressed.

The regressions to the PCs of the second modes of precipitation and SSTs for the JJA season (Figure 6(d) and (h)) show that in years when the SSTs are above normal in the northern Indian Ocean and the warm pool and below normal in the mid-latitude western Pacific (Figure 5(d)), a strong north–south dipole of height anomalies forms, with negative to the north of 30 °N and positive to the south of 30 °N. From the south, anomalous southeasterly flow enhances the climate-mean southeast monsoon winds and brings more warm and moist air to central eastern China. From the north, anomalous southerly flow weakens the climate-mean monsoon winds and brings down cold and dry air. The two branches of anomalous flow converge over central eastern China and produce above-normal precipitation.

In this section the dynamical links between the anomalous SSTs and China precipitation were explored through regression analyses. The SSTs over the warm pool and northern Indian Ocean play a key role in modulating the strength and displacement of the western Pacific subtropical high (e.g. Huang and Lu, 1989; Wu *et al*., 2003). The corresponding anomalous monsoonal flow affects the direction and strength of the transport of water vapour into East China and, consequently, affects the interannual variability of precipitation over this region.

5. DECADAL VARIATIONS AND TRENDS

So far we have analysed the interannual variability of China precipitation in boreal spring and summer and its associated monsoon circulation, and found that variations of China precipitation consist of a few well-defined modes that are linked to SSTs in different oceanic regions. On a longer time scale, both the observed precipitation and SSTs exhibit decadal variations and long-term trends (Figures 2–4). Weng *et al*. (1999) applied SVD analyses to unfiltered precipitation and SSTs to document the coupled modes of SST and precipitation in JJA. They did not separate the interannual variations from the interdecadal components. In this section we address the question of whether the modes of China precipitation on the decadal time scale are different from those at the interannual time scale. Previous studies (e.g. Trenberth and Hurrell, 1994; Zhang *et al*., 1997) have showed that the dominant SST modes, such as the ENSO and North Pacific mode, consist of variations with period ranging from seasons to decades. Can the observed decadal variations and trends of China precipitation be explained by the decadal variations of SSTs?

We first performed matrix operations by multiplying the observed unfiltered seasonal mean precipitation and SST anomalies with the respective leading SVD modes of precipitation and SSTs shown in Figure 5 for each season. The resulting time series, referred to as projections to the SVD modes, illustrate to what degree the observed anomaly in a given year is associated with the dominant interannual SVD modes. The projections of SST anomalies to the first two leading SST modes are shown in Figure 7 as bars for each mode and each season. The lines in Figure 7 are 7 year running means of the projections. On the interannual time scale, the projections resemble the corresponding PCs of the leading SST modes in both MAM and JJA (not shown). The first projections (PJ1_SST) in both MAM and JJA capture the major cold and warm events in the tropical Pacific and Indian Ocean. The second projections (PJ2_SST) reflect primarily SST variations over the warm pool and Indian Ocean. However, unlike the PCs, these projections, except for PJ2_SST in MAM, all demonstrate a distinct upward trend in the 48 year period from 1951 through to 1998, with the turning point occurring in the mid 1970s. The trends indicate a basin-wide warming of SSTs in the tropics.

The projections of precipitation anomalies to the first two leading modes of precipitation are presented in Figure 8. On the interannual time scale these projections also resemble the corresponding PCs of precipitation (not shown). Unlike the PCs, interdecadal variations and trends are superimposed on the interannual variations

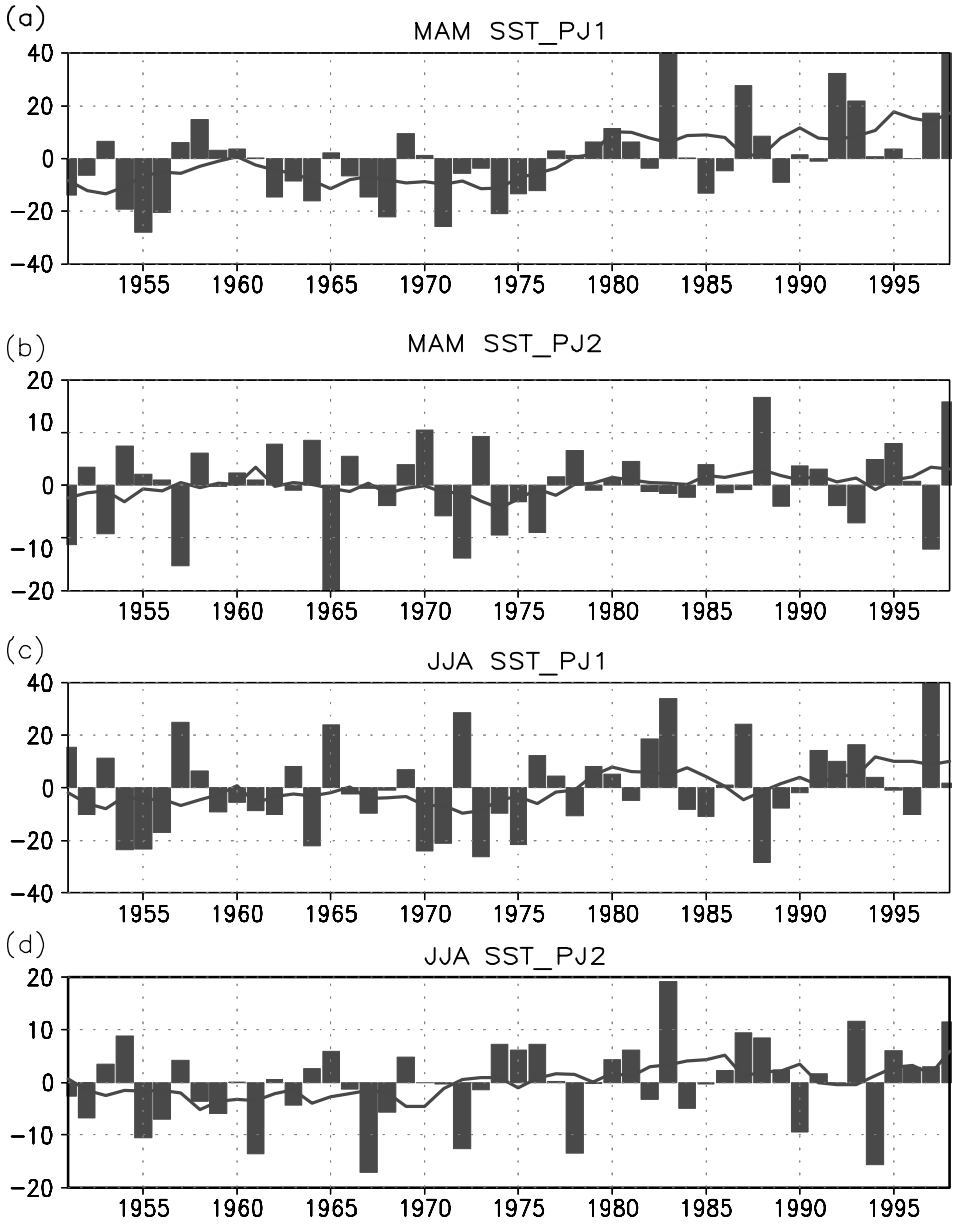

Figure 7. Projections of the observed unfiltered SST anomalies in MAM and JJA to the SVD modes of SSTs as illustrated in Figure 5. The projection is defined as a matrix product between each SVD mode and the seasonal mean unfiltered SST anomalies over the same domain given by SVD mode. The lines are 7 year running means of the projections

of the projections. PJ1 in MAM and PJ2 in JJA show upward trends of precipitation and PJ2 in MAM and PJ1 in JJA show downward trends.

In comparison with the area-mean anomalies of precipitation shown in Figure 3, the projections of precipitation (Figure 8) exhibit some interesting features. In MAM, PJ1 matches the 'south China' mean and PJ2 matches the 'central China' mean. In JJA, PJ1 matches the 'north China' mean, and PJ2 the 'central China' mean. These projections and area-means match each other in the sense that they possess not only similar interannual variations but also have almost identical interdecadal variations for the 48 year period. Referring to the leading modes of precipitation shown in Figure 5, we propose that the observed precipitation trends over the different areas of East China and in different seasons during the 1951–98 period are a manifestation of the

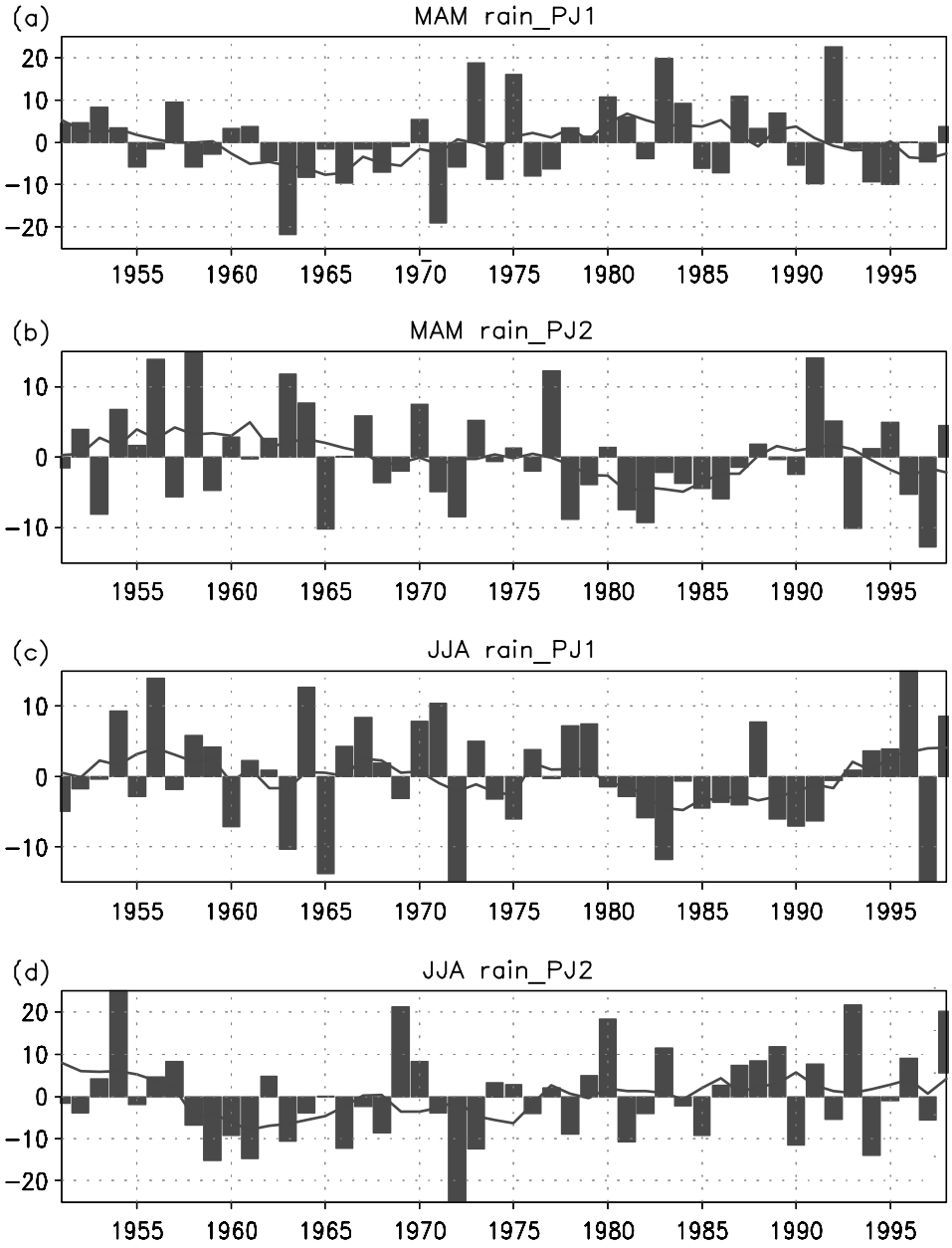

Figure 8. As Figure 7, except for precipitation

long-term variations in the strength and polarization of those dominant interannual precipitation modes. Given the fact that the interannual modes of precipitation are covarying with the dominant interannual modes of SSTs identified by SVD in Section 3, and that those interannual modes of SSTs also posses decadal variations and trends (Figure 7), we further propose that the observed long-term variations of precipitation over East China are likely forced by the decadal variations of the dominant interannual SST modes. The more frequent floods over southeastern China in MAM and severe droughts over northern China in JJA in recent decades are associated with the upward trend of SSTs associated with the ENSO-like mode (Figure 5(a) and (c)). The recent frequent flooding events in JJA over central eastern China are linked to the trend of the second mode

of SSTs, which reflects primarily the SST variations over the northern Indian Ocean and the warm pool. The case for the upward trend of precipitation over central eastern China in MAM is an exception, for which the explanation follows.

For the precipitation over central eastern China in MAM, the SVD analysis in Section 3 indicates that, on the interannual time scale, precipitation is positively correlated with the SSTs over the Indian Ocean and the warm pool (Figure 5(b)). Whereas in MAM the projection of precipitation anomalies to the second mode of precipitation (Figure 8(b)) shows a downward trend that resembles the evolution of the observed 'central China' precipitation (Figure 3(b)), the projection of SST anomalies in MAM to the second SST mode (Figure 7(b)) actually shows a weak upward trend. These seemly contradictory relationships suggest that over central eastern China the decadal variation of precipitation in MAM may not be associated with the interannual mode identified by the SVD analysis using the high-pass filtered data.

To test this possibility, we first separate each time series of the area-mean precipitation anomalies shown in Figure 3 into interannual and decadal components by applying a digital filter with a 7 year cutoff period. Then we correlated the interannual and the decadal time series with the corresponding 7 year high- and low-pass filtered SSTs, respectively, at each oceanic grid point. The computed anomalous correlations are presented in Figure 9 for the cases of 'south China' and 'central China' in MAM and 'central China' and 'north China' in JJA. There is a distinct contrast between the high-pass and low-pass correlation maps for the 'central China' case in MAM compared with the other three cases. For the cases of 'south China' in MAM and 'central China' and 'north China' in JJA, the pair of the high-pass and low-pass correlation maps resemble each other, and are both similar to the corresponding SST modes in Figure 5 in terms of pattern distributions. The result reinforces the notion that, for these cases, the interannual and decadal variations of precipitation over each region and for each season are controlled by a single precipitation mode, which is linked to the same mode of SSTs as suggested by Weng *et al*. (1999). However, for the 'central China' case in MAM, the high-pass correlation map (Figure 9(b)) is totally different from the low-pass correlation map (Figure 9(f)). The former resembles the interannual SST mode in Figure 5(b), and the latter resembles the long-term SST trend in Figure 4(a). Therefore, in MAM over central eastern China there are two precipitation modes operating at different time scales. The interannual mode is forced by, and positively correlated with, the interannual modes of SSTs over the Indian Ocean and the warm pool (Figure 5(b)). The decadal mode is forced by, and negatively correlated with, the basin-wide decadal variations of SSTs in the entire Indian and Pacific Oceans (Figure 9(f)). The observed downward trend of precipitation over central eastern China in MAM (Figure 3(b)) is linked to the basin-wide warming trend of SSTs (Figure 4(a)).

We further test the above hypothesis by repeating the SVD analysis described in Section 3 with unfiltered seasonal mean precipitation and SST anomalies. The resulting modes are presented in Figure 10 and the percentage variances explained by each mode and the correlations between the PCs are listed in Table II. For JJA, the two leading modes of SSTs (Figure 10(c) and 10(d)) and precipitation (Figure 10(g) and 10(h)) are almost identical to those shown in Figure 5. The resulting PCs (Figure 11(c) and 11(d)) are similar to the PCs corresponding to Figure 5 (not shown) in terms of interannual variability, but possess obvious interdecadal variations and trends, which match the projections in JJA shown in Figure 7 for SSTs and in Figure 8 for precipitation and the observed precipitation trends in Figure 3(c) and (d). Similar relationships can be obtained for the first SVD modes of precipitation and SSTs for MAM (Figure 10(a) and 10(e)). The second SST mode in MAM (Figure 10(b)), however, is different from the interannual mode derived from the high-pass filtered data (Figure 5(b)). This SST mode reflects SST variations primarily in the North Pacific. The PCs of SSTs and precipitation are negatively correlated ($r = -0.61$) (Figure 11(b)). The PC of SSTs depicts a general upward trend and the PC of precipitation shows a downward trend. This analysis further confirms that the forcing mechanism for the observed precipitation trend over central eastern China in MAM is different from that for other cases. Hence, there are two different modes of SSTs operating at different time scales that control the precipitation variability over central eastern China in MAM.

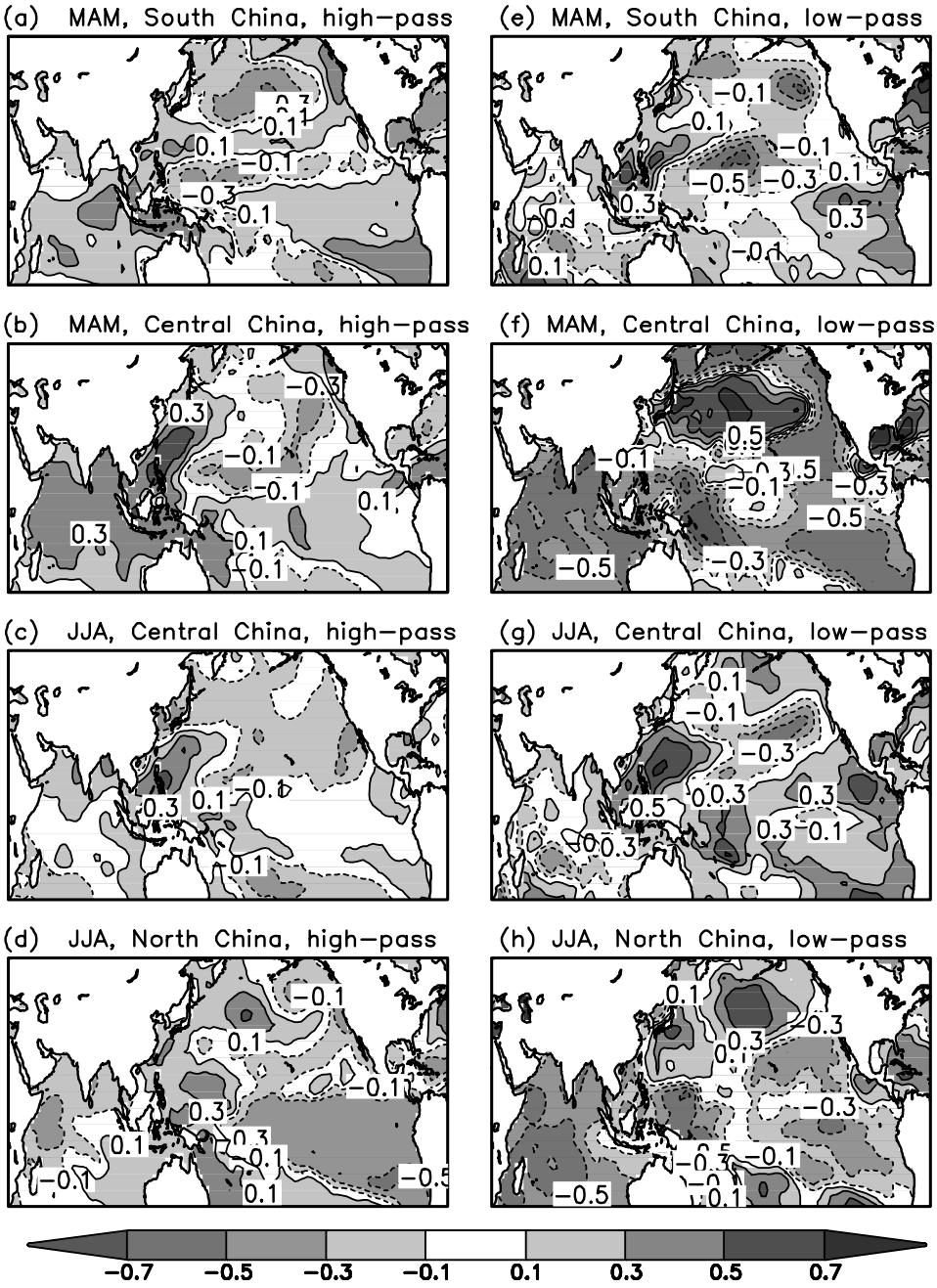

Figure 9. Correlations between high- and low-pass-filtered regional mean precipitation in Figure 3 and the corresponding filtered SST anomalies. Left panels are for the 7 year high-pass filtered data, and right panels for the 7 year low-pass filtered data. See text for the details

6. SUMMARY AND DISCUSSION

6.1. Summary

In this study we documented the variability of China precipitation in boreal spring and summer and its links to global SSTs. Starting from the assumption that the modes of precipitation at the interannual and decadal

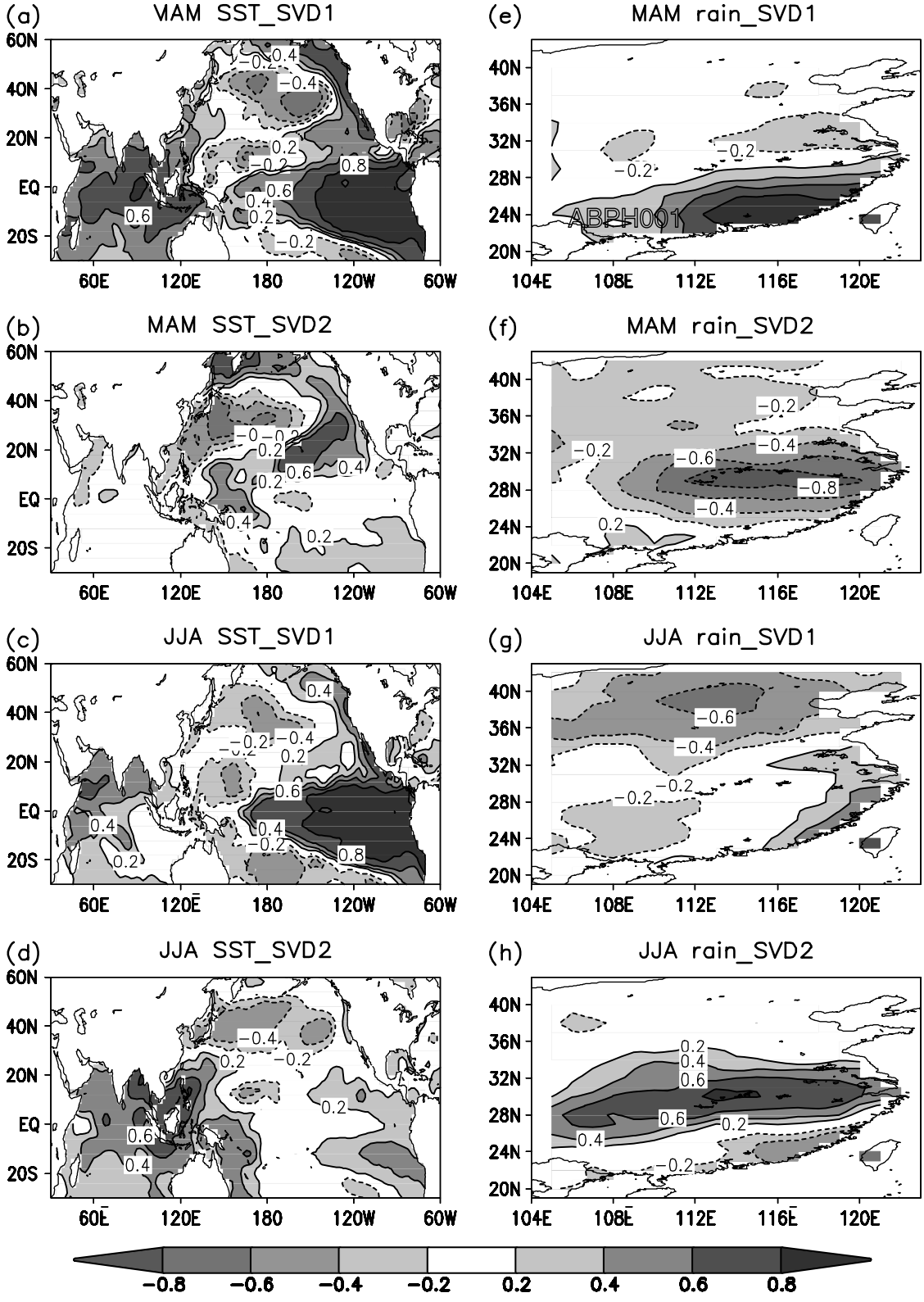

Figure 10. As Figure 5, except that the modes are derived from unfiltered SSTs and precipitation

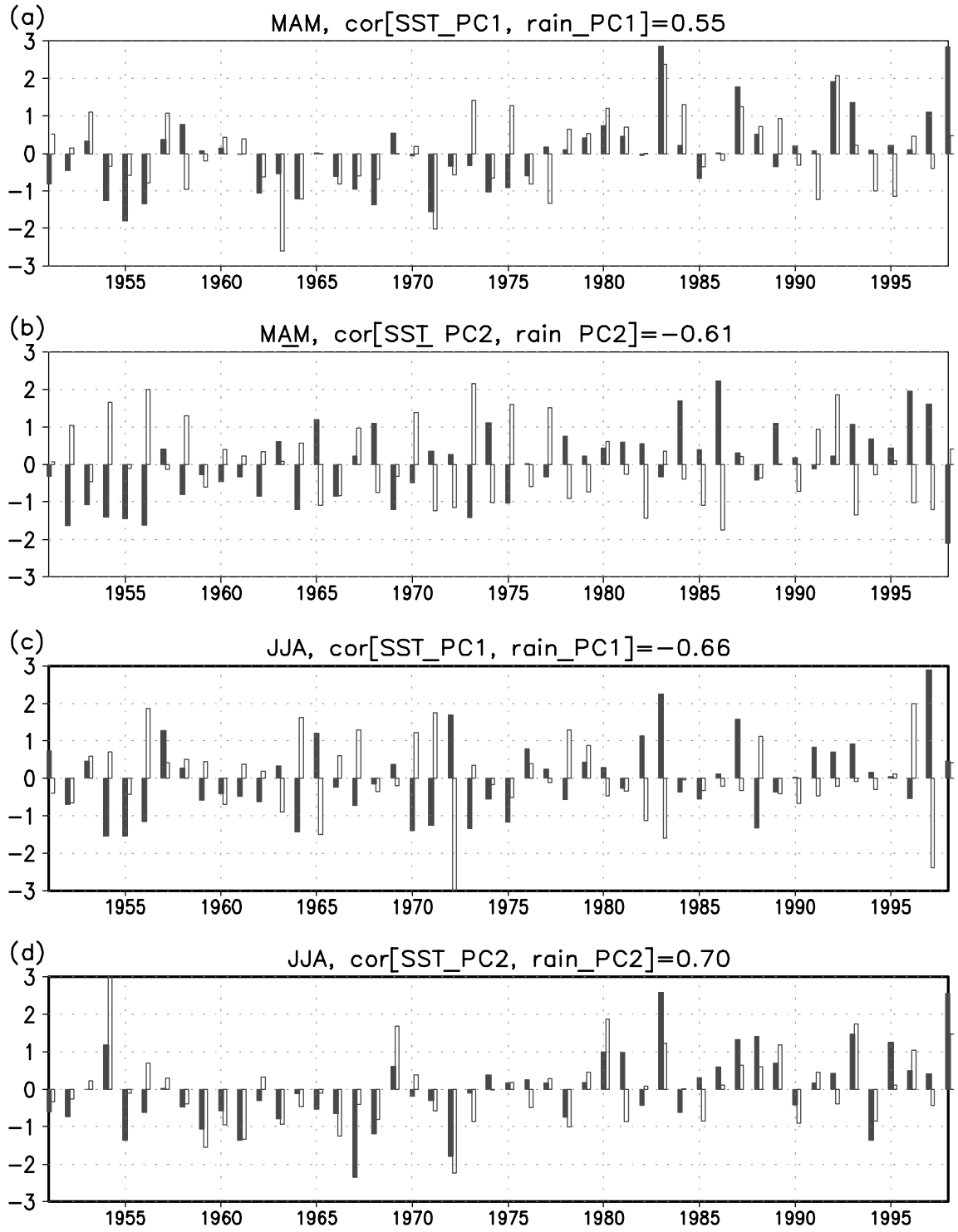

Figure 11. PCs for the first two leading SVD modes derived from unfiltered SSTs and precipitation as shown in Figure 10. The PCs for the SST modes are solid bars, and those for the precipitation modes are unshaded bars. Each PC is normalized by its own standard deviation. The correlation between the pair of PCs in each panel is displayed

time scales are not necessarily the same and that they might be associated with different modes of SSTs, we first applied SVD analysis to the high-frequency-pass filtered precipitation and SST anomalies to identify the coupled modes of precipitation and SSTs on the interannual time scale. Results show that a large portion of the East China precipitation variance at the interannual time scale can be explained by two centres of action for each season, which are covarying with two interannual modes of SSTs. The leading SVD modes of precipitation in spring and summer, which are centred in southeastern China and northern China respectively, are both linked to an ENSO-like mode of SSTs. In years when the central and eastern tropical Pacific and Indian Ocean are abnormally warm, precipitation tends to be above normal over southeastern China in MAM and below normal over northern China in JJA. The second SVD modes in both seasons reflect the interannual variability of precipitation over central eastern China, and are linked primarily to SST variations over the warm pool and Indian Ocean. In years when SSTs over these regions are abnormally warm, central eastern China tends to have more precipitation in both seasons. Further analyses of anomalous 850 hPa winds and 700 hPa geopotential heights corresponding to these modes support a physical mechanism that explains the causal links between the main variations of precipitation and SSTs.

Results based on projection, point correlation and SVD using unfiltered datasets show that, by and large, the coupled modes of precipitation and SSTs at the interannual time scale identified using filtered data also operate on the decadal time scale. Hence, the interannual and interdecadal variations of precipitation can be explained by the same mode of SSTs. The upward trend of springtime precipitation over southeastern China and downward trend of summertime precipitation over northern China are linked to the warming trend of the ENSO-like SST mode. The recent frequent summertime floods over central eastern China are linked to the warming trend of SSTs over the warm pool and Indian Ocean. The exceptional case is for the springtime precipitation over central eastern China. For this case, whereas the interannual mode of precipitation is positively correlated with SSTs over the warm pool and Indian Ocean, the interdecadal mode is negatively correlated with a different SST mode, i.e. the North Pacific mode. The latter is responsible for the observed downward trend of springtime precipitation over central eastern China.

6.2. Discussion

This study only investigated the contributions of SSTs to the observed trends and variability of China precipitation. Not all the variances of precipitation can be explained by SSTs. It is possible that other factors, such as snow cover and polar ice concentration, also play a role. A recent study by Menon *et al*. (2002) further suggests that the observed trends of China precipitation in recent decades are forced by the increase of black carbon emissions over South and East Asia.

The links between precipitation and SSTs identified in the present study do not necessarily prove a cause-and-effect relationship. On the interannual time scale, SSTs over the warm pool and South China Sea are often influenced by strong anomalous monsoon circulation. Air–sea interaction can modulate the local SSTs (Wang *et al*., 2003). The monsoon–ENSO relation is far more complicated than which we have attempted to address here. Anomalous monsoon circulation can affect the evolution or even trigger ENSO events. Barnett (1984) noted that, on the interannual time scale, the Asian monsoon and ENSO are strongly coupled through the propagation of anomalous atmospheric circulation from the Indian to the Pacific sector. Shen and Lau (1995) found a strong biennial signal in the correlations between the East Asian summer monsoon and the tropical SSTs. The present study suggests that precipitation over central eastern China is strongly coupled with SSTs over the western tropical Pacific and Indian Ocean. SST anomalies over these regions, to a certain degree, are related to ENSO, but also are independent of it. We further examined the PCs corresponding to Figure 5 for extreme events, and found that in El Niño (La Niña) years the precipitation is almost always above (below) normal over southeastern China in MAM and below (above) normal over northern China in JJA. However, ENSO events and extreme precipitation seasons do not match in all years. The effect of ENSO on precipitation over central eastern China is far less conclusive.

For the changes in decadal and longer time scales, a regime shift has been identified for the relationship between the Indian monsoon and ENSO (Kumar *et al*., 1999; Krishnamurthy and Goswami, 2000; Kinter *et al*., 2002). The relationship between East Asian climate and ENSO also experienced a regime shift in the

mid-1970s (Kinter *et al*., 2002; Wang, 2001), although the mechanism of this is still not understood. It is possible that the observed trends in both precipitation and SSTs identified in the present study are merely a manifestation of the regime shift. There is also the possibility that global warming might have affected the precipitation patterns over China by directly changing the Asian monsoon dynamics and indirectly modifying the Eurasian snow cover and the polar ice concentration. By comparing observations with results from simulations of transient greenhouse warming by 16 coupled atmosphere–ocean GCMs, Hu *et al*. (2003) found that the observed long-term temperature variations over China in all seasons but summer may be associated with increases in greenhouse gas concentrations. Owing to the large uncertainties among the GCMs in precipitation simulations, they did not find a robust link between the precipitation variations and global warming. The present study may provide a working hypothesis for further investigations to understand better the variability and trends of China precipitation.

ACKNOWLEDGEMENTS

We thank two anonymous reviewers for their constructive and insightful comments. This research was partially supported by the NASA Modeling, Analysis and Prediction program.

REFERENCES

Barnett TP. 1984. Interaction of the monsoon and Pacific trade wind system at interannual time scales. Part III: a partial anatomy of the southern oscillation. *Monthly Weather Review* **112**: 2388–2400.

Bretherton CS, Smith C, Wallace JM. 1992. An intercomparison of methods for finding coupled patterns in climate data. *Journal of Climate* **5**: 541–560.

Cherry S. 1997. Some comments on singular value decomposition analysis. *Journal of Climate* **10**: 1759–1761.

Chang CP, Zhang Y, Li T. 2000. Interannual and interdecadal variations of the East Asian summer monsoon and tropical Pacific SSTs. Part I: role of the subtropic ridge. *Journal of Climate* **13**: 4310–4325.

Chen L, Dong M, Shao Y. 1992. The characteristics of interannual variation on the East Asian monsoon. *Journal of the Meteorological Society of Japan* **70**: 397–421.

Chen M, Xie P, Janowiak JE, Arkin PA. 2002. Global land precipitation: a 50-yr monthly analysis based on gauge observations. *Journal of Hydrometeorology* **3**: 249–266.

Ding YH. 1992. Summer monsoon rainfalls in China. *Journal of the Meteorological Society of Japan* **70**: 373–396.

Duchon CE. 1979. Lanczos filtering in one and two dimensions. *Journal of Applied Meteorology* **18**: 1016–1022.

Gong DY, Ho CH. 2002. Shift in the summer rainfall over the Yangtze River valley in the late 1970s. *Geophysical Research Letters* **29**: 1436. DOI: 10.1029/2001GL014523.

Hu Q. 1997. On the uniqueness of the singular value decomposition in meteorological applications. *Journal of Climate* **10**: 1762–1766.

Hu ZZ. 1997. Interdecadal variability of summer climate over East Asia and its association with 500 hPa height and global sea surface temperature. *Journal of Geophysical Research* **102**: 19 403–19 412–.

Hu ZZ, Yang S, Wu R. 2003. Long-term climate variations in China and global warming signals. *Journal of Geophysical Research* **108**: 4614. DOI: 10.1029/2003JD003651.

Huang R, Lu L. 1989. Numerical simulation of the relationship between the anomaly of subtropical high in East Asia and the convective activities in the tropical western Pacific. *Advances in Atmospheric Sciences* **6**: 202–214.

Huang R, Wu Y. 1989. The influence of ENSO on the summer climate change in China and its mechanism. *Advances in Atmospheric Sciences* **6**: 21–32.

Huang R, Zhang R, Zhang Q. 2000. The 1997/98 ENSO cycle and its impact on summer climate anomalies in East Asia. *Advances in Atmospheric Sciences* **17**: 348–362.

Ju JH, Slingo J. 1995. The Asian summer monsoon and ENSO. *Quarterly Journal of the Royal Meteorological Society* **121**: 1133–1168.

Kalnay E, Kanamitsu M, Kistler R, Collins W, Deaven D, Gandin L, Iredell M, Saha S, White G, Woollen J, Zhu Y, Chelliah M, Ebisuzaki W, Higgins W, Janowiak J, Mo KC, Ropelewski C, Wang J, Leetmaa A, Reynolds R, Jenne R, Joseph D. 1996. The NCEP/NCAR 40-year reanalysis project. *Bulletin of the American Meteorological Society* **77**: 437–471.

Kinter III JL, Miyakoda K, Yang S. 2002. Recent change in the connection from the Asia monsoon to ENSO. *Journal of Climate* **15**: 1203–1215.

Krishnamurthy V, Goswami BN. 2000. Indian monsoon–ENSO relationship on interdecadal time scale. *Journal of Climate* **13**: 579–595.

Kumar KK, Rajagopalan B, Cane MA. 1999. On the weakening relationship between Indian monsoon and ENSO. *Science* **284**: 2156–2159.

Lau KM, Weng H. 2001. Coherent modes of global SST and summer rainfall over China: an assessment of the regional impacts of the 1997–98 El Niño. *Journal of Climate* **14**: 1294–1308.

Lau KM, Yang S. 1997. Climatology and interannual variability of the Southeast Asian summer monsoon. *Advances in Atmospheric Sciences* **14**: 141–162.

Menon S, Hansen J, Nazarenko L, Luo YF. 2002. Climate effects of black carbon aerosols in China and India. *Science* **297**: 2250–2253.

New M, Hulme M, Jones P. 2000. Representing twentieth-century space–time climate variability. Part II: development of 1901–96 monthly grids of terrestrial surface climate. *Journal of Climate* **13**: 2217–2238.

Newman M, Sardeshmukh P. 1995. A caveat concerning singular value decomposition. *Journal of Climate* **8**: 352–360.

Nitta T, Hu ZZ. 1996. Summer climate variability in China and its association with 500 hPa height and tropical convection. *Journal of the Meteorological Society of Japan* **74**: 425–445.
Shen S, Lau KM. 1995. Biennial oscillation associated with the East Asian summer monsoon and tropical sea surface temperature. *Journal of the Meteorological Society of Japan* **73**: 105–124.
Tao SY, Chen LX. 1987. A review of recent research of the East Asian summer monsoon in China. In *Monsoon Meteorology*, Chang CP, Krishnamurti TN (eds). Oxford University Press: 60–92.
Trenberth KE, Hurrell JW. 1994. Decadal atmosphere–ocean variations in the Pacific. *Climate Dynamics* **9**: 303–319.
Wang B, Wu R, Lau KM. 2001. Interannual variability of the Asian summer monsoon: contrasts between the Indian and the western North Pacific–East Asian monsoons. *Journal of Climate* **14**: 4073–4090.
Wang B, Wu R, Fu X. 2000. Pacific–East Asian teleconnection: how does ENSO affect East Asian climate. *Journal of Climate* **13**: 1517–1536.
Wang B, Wu R, Li T. 2003. Atmosphere–warm ocean interaction and its impacts on Asian–Australian monsoon variation. *Journal of Climate* **16**: 1195–1211.
Wang WC, Li KR. 1990. Precipitation fluctuation over semiarid region in northern China and the relationship with El-Nino southern oscillation. *Journal of Climate* **3**: 769–783.
Wang HJ. 2001. The weakening of the Asian monsoon circulation after the end of 1970's. *Advances in Atmospheric Sciences* **18**: 376–386.
Webster PJ, Magana VO, Palmer TN, Shukla J, Tomas RA, Yanai M, Yasunari T. 1998. Monsoons: processes, predictability, and the prospects for prediction. *Journal of Geophysical Research* **103**: 14 451–14 510–.
Weng H, Lau KM, Xue Y. 1999. Multi-scale summer rainfall variability over China and its long-term link to global sea surface temperature variability. *Journal of the Meteorological Society of Japan* **77**: 845–857.
Wu R. 2002. A mid-latitude Asian circulation anomaly pattern in boreal summer and its connection with Indian and East Asian summer monsoons. *International Journal of Climatology* **22**: 1879–1895.
Wu R, Hu ZZ, Kirtman BP. 2003. Evolution of ENSO-related rainfall anomalies in East Asia. *Journal of Climate* **16**: 3741–3757.
Wu R, Kinter III JL, Kirtman BP. In press. Discrepancies of interdecadal changes in the Asian region between NCEP–NCAR reanalysis and observations. *Journal of Climate*.
Xue Y, Smith TM, Reynolds RW. 2003. Interdecadal changes of 30-yr SST normals during 1871–2000. *Journal of Climate* **16**: 1601–1612.
Zhang Y, Wallace JM, Battisti DS. 1997. ENSO-like interdecadal variability: 1990–1993. *Journal of Climate* **10**: 1004–1020.

